SPIONs magnetic nanoparticles for MRI applications: Microwave synthesis and physicochemical, magnetic and biological characterizations

Thomas Girardet, Emilie Bianchi, Christel Henrionnet, Astrid Pinzano, Sabine Bouguet-Bonnet, Corentin Boulogne, Sebastien Leclerc, Franck Cleymand, Solenne Fleutot

SPIONs magnetic nanoparticles for MRI applications: microwave synthesis and physicochemical, magnetic and biological characterizations †

Thomas Girardet [a], Emilie Bianchi [a], Christel Henrionnet [b], Astrid Pinzano [b], Sabine Bouguet-Bonnet [c], Corentin Boulogne [c], Sébastien Leclerc [d], Franck Cleymand [a] and Solenne Fleutot [a*]

a Institut Jean Lamour, CNRS, Université de Lorraine, F-54000 Nancy, France

b IMoPA, Université de Lorraine, F-54000 Nancy, France

c CRM², Université de Lorraine, F-54000 Nancy, France

d LEMTA, Université de Lorraine, F-54000 Nancy, France

† Electronic Supplementary Information (ESI) available: XRD, FTIR, TGA, magnetic characterizations and relaxometry at 20 MHz, 40 MHz and 60 MHz, table S1.

* corresponding author: solenne.fleutot@univ-lorraine.fr

Abstract

More and more biomedical applications used nanoparticles to improve their quality and their possibilities. Among the nanoparticles used, Superparamagnetic Iron Oxide Nanoparticles (SPIONs) are often used because these nanoparticles are biocompatible, non-toxic and the ease of synthesizing them. The aim of this study is to obtain highly water-soluble iron oxide nanoparticles using a microwave process. The SPIONs developped with this technique have a diameter between 2 nm to 4 nm range, are monodisperse and stable in an aqueous media. Indeed, with the microwaves, the control of the temperature is more precise and allows so to obtain nanoparticles with a same diameter. After the synthesis, several characterizations are carried out to determine the shape, the size, the chemical composition, the stability and the magnetic properties. Then, these SPIONs can use to control the regeneration of tissues such as cartilage tissue. For that, SPIONs are internlasized in mesenchymal stromal cells (MSCs) because these cells can to differenciate into all humans cells and allows so to regenerate all tissues: these cells are good candidate for tissue engineering. In this work, the internalization of SPIONs and the cytotocixity are studied and confirm the biocompatibility of our SPIONs. Then, for the control of the regeneration of tissues, relaxometry and MRI (Magnetic Resonance Imaging) of SPIONs are realized to compare with the commercial contrast agent present (Endorem®). For our SPIONs, the values of transverse and longitudinal relaxivities are high and in the same order to Endorem®.

Keywords: iron oxide nanoparticles, microwave assisted synthesis, MTT tests, relaxometry measurements, MRI, NMRD profils

1. Introduction

Magnetic nanoparticles, and especially iron oxide nanoparticles, are used often in biomedical applications such as hyperthermia, drug delivery, contrast agents, etc [1–5]. In function of the size,

iron oxide nanoparticles will have different magnetic properties: for a spherical nanoparticle, if the size is higher to 20 nm, nanoparticles will have a ferrimagnetic behaviour [6]. However, if the size is lower than 20 nm, iron oxide nanoparticles will have a superparamagnetic state: this magnetic state is important for different imageries such as Magnetic Resonance Imaging (MRI) [7–9], Magnetic Particle Imaging (MPI) [10–12] or a combination of other medical imaging with for example Positron Emission Tomography (PET) [13–15]. However, these last imaging techniques (PET/MPI) are used for a diagnostic imaging instead of MRI is used to obtain anatomical information.
Due to their superparamagnetic behaviour and their biocompatible nature, Superparamagnetic Iron Oxide Nanoparticles (SPIONs) are good candidates for these imagery techniques. These SPIONs should have several optimum physico-chemical properties for biomedical applications: size and a narrow size distribution, stable in an aqueous solution, good magnetic properties.
To obtain SPIONs with these properties, there exists different synthesis with each advantage and disadvantages. For example, thermal decomposition is a good synthesis to obtain SPIONs with a good crystallinity, a control of the size, the shape and the size distribution [7,16–18]. The disadvantage of this synthesis is the presence of an organic solvent: another step to remove the organic solvent is obligatory for the biomedical applications [19,20].

To overcome this problem, a synthesis directly in water can be done: it's the coprecipitation synthesis. This synthesis is the most used because nanoparticles are easily and quickly obtained [21–23]. To synthesise SPIONs, a mixture of iron salts (generally iron chloride II and iron chloride III) with a base (ammonium hydroxide) is realized [24]. However, the control of the shape, size and the size distribution is very difficult and aggregation phenomena occur [25]. In order to isolate SPIONs, a functionalization step is necessary with organic or/and inorganic shells [26–29].
To control the size, the shape, the size distribution and magnetic properties directly in an aqueous solution, a new synthesis method is more and more used: microwave synthesis [30,31]. Indeed, thanks to microwave irradiations, there is a control of the temperature inside the reactor (the temperature gradient between the walls of the reactor and the interior is minimal) thus allowing a better control of the physico-chemical parameters [32]. In addition, this process allows synthesizing a high quantity of SPIONs with a very good yield in a short time.

This synthesis method coupled to a functionalization by a ligand allows to obtain SPIONs which are stable in an aqueous solution with a good control of the size, the shape and the size distribution.
The goal of these nanoparticles is to use these for the biomedical applications such as MRI. However, before to obtain MRI images, a study of the SPIONs behaviour with cells is important. For this, an internalization of SPIONs in mesenchymal stromal cells (MSCs) is carried out. Indeed, these cells provide a large possibility to regenerate damaged tissues in articular diseases thanks to their large differentiation potentialities [33]. With SPIONs inside MSCs, a follow-up of the cartilage regeneration is possible through the MRI.

To increase the quality of images in MRI, contrast agents are increasingly used. Indeed, they allow to decrease the examination time, to quickly and easily distinguish between healthy and diseased tissues and to provide more information on the functioning of the organs [9]. There exist two types of contrast agent: positive contrast agent and negative contrast agent. The positive contrast agents are composed of a paramagnetic center (such as Gd^{3+}, Mn^{2+} [34,35]). They can shorten the longitudinal relaxation time (T_1). In addition, the contrast agent with a Gd^{3+} complex can cause a toxicity if the cation is free

on a living organism [36]: the goal with these contrast agents is to chelate the paramagnetic centre or to use another cation such as Mn^{2+}. For the negative contrast agents, they are composed of a superparamagnetic center (iron oxide nanoparticles for example): they can shorten the transverse relaxation time (T_2), which allows a reduction in the intensity of the signal [37,38]. To increase this transverse relaxation, several commercial contrast agents, such as Endorem®, Ferumoxides®, were used in clinical MRI. These contrast agents are SPIONs with an inorganic core diameter around 5 nm and a hydrodynamic diameter around 100-150 nm.

The goal of this study is to synthesise SPIONs with the microwave synthesis. After the synthesis, systematic characterizations were realized to determine the shape, the size, the chemical composition, the stability and the magnetic properties. Then, after a sterilisation step, a study of the internalisation of SPIONs in cells as well as a study of the cytotoxicity are carried out to check if these nanoparticles are biocompatible in human cells. Finally, to verify if these nanoparticles have a good signal in MRI and to determine the best conditions to use it, relaxometry measures and MRI images were performed.

2. Materials and methods

2.1 Materials

Ferrous chloride ($FeCl_2.4H_2O$) and ferric chloride ($FeCl_3.6H_2O$) were purchased from Alfa Aesar. Citric acid ($C_6H_8O_7$), absolute ethanol (99%) and ammonium hydroxide solution (NH_4OH) were purchased from Sigma Aldrich. In all experiment, ultrapure water (resistivity = 18.2 MΩ.cm) was used.

2.2 Synthesis

A solution of ferrous chloride ($FeCl_2.4H_2O$; 5.03 mmol) and ferric chloride ($FeCl_3.6H_2O$; 3.7 mmol) with citric acid ($C_6H_7O_8$; 3.16 mmol) in 15 mL of ultra-pure water is realized in a Pyrex reactor for the microwave. Then, 5 mL of ammonium hydroxide solution (NH_4OH) is added to precipitate the solution: the solution turns black and it is placed in the microwave reactor. The microwave is a single mode microwave (Monowave 400) from Anton Paar which operates at a frequency of 2.45 GHz and with a maximum power of 850W.

The solution is heating at 96°C for 40 min. The synthesis parameters are optimised by a design experiment. After heating, the solution is collected and washed by centrifugation with different solvents. The first step is a mixture of absolute ethanol and the nanoparticles solution which is centrifuged during 5 min at 10 000 rpm. The last step is another centrifugation during 5 min at 10 000 rpm with a mixture of ultrapure water and absolute ethanol. Finally, SPIONs obtained are dispersed in ultrapure water. A part is evaporated at 60°C in an oven to obtain powder for some characterization techniques. The other part stays in liquid state for TEM, DLS and FTIR analysis. For this study, three experiments are presented: one which has the optimised parameters (SPIONs_CA1) and two which come from the design experiment (SPIONs_CA2 and SPIONs_CA3). The difference of the synthesis between SPIONs_CA1 and CA2 is the temperature rape time: 5min for SPIONs_CA2 and 10min for SPIONs_CA1. For SPIONs_CA3, the difference with SPIONs_CA1 is a higher temperature of synthesis (110°C instead of 96°C).

2.3 Characterizations techniques

Different techniques are used to control the physico-chemical parameters of SPIONs.

2.3.1 Transmission Electron Microscopy

Transmission Electron Microscopy (TEM) is used to analyse the size, the size distribution, and the shape of SPIONs. The TEM is a CM200-FEI operating at 200 kV (point resolution 0.27 nm). A drop of the solution was deposit on a copper grid with a carbon film and dried to evaporate the solvent. After the analysis, the size distribution is calculated using free software ImageJ.

2.3.2 Dynamic Light Scattering

Dynamic Light Scattering (DLS) was performed by the ZETASIZER Nano ZS device from Malvern Panalytical. The solution of SPIONs obtained after the synthesis is diluted to obtain a solution with a concentration of 0.2 mg/mL. Thanks to the DLS measurements, the hydrodynamic diameter and the stability of SPIONs in the solution can be determined. DLS measurements are performed three times and the average of these three measurements will be presented in this study.

2.3.3 X-Ray Diffraction

X-Ray Diffraction (XRD) patterns were recorded in standard conditions with an INEL CPS120 equipped with a monochromatic cobalt radiation (Co Kα = 0.17886 nm) at grazing angle of incidence simultaneously at 120°.

2.3.4 Fourier Transform Infra-Red

Fourier Transform Infra-Red Spectroscopy (FTIR) was performed with a Nicolet 6700 from Thermo-Fisher between 400 and 4000 cm^{-1} with a resolution of 4 cm^{-1} and an accumulation of 256 scans for each spectrum.

2.3.5 Thermogravimetric analysis

Thermogravimetric analysis (TGA) was performed on SPIONs powder to determine the quantity of the organic shell and of the iron oxide core. The device used was a SETSYS EV 1750 TGA microbalance from Setaram. Experiments were conducted in the temperature range of 20-600°C under air flow (20 mL/min) at a heating rate of 10°C/min.

2.3.6 Magnetic measurements

A Superconducting Quantum Interference Device (SQUID) with a Vibrating Sample Magnetometer (VSM) from Quantum Design is used to determine the saturation magnetization (Ms) and the blocking

temperature (T_B). The magnetic field which is applied sweeps from +5 T to -5 T and then from -5 T to +5 T.
For the Zero Field Cooled/Field Cooled (ZFC/FC) curves, the sample was cooled to 5K without magnetic field. After, a magnetic field of 0.02 T is applied and the temperature heats from 5K to 300K (ZFC curve). Finally, the sample was cooled down to 5K (FC curve).

2.3.6 Ethics statement, isolation and culture of human bone mesenchymal stroma cells (MSCs)

MSCs were isolated from femoral necks of patients undergoing total hip replacement (all bone samples were received from our local bone bank, UTCT). The MSCs obtained were anonymous when researchers received them. These experiments with MSCs were approved ethically and methodologically by the local Research Institution (Direction de la Recherche et de l'Innovation registration number UF 9757 – Contrat de Programme de Recherche Clinique – Cellules souches et chondrogenèse). These studies were conducted with informed patients (written consent, non-opposition) in accordance with the usual ethical legal regulations (decrees n2007-1220 and AC-2008-49). All procedures were done in accordance with our authorization and registration number DC-2008-263 given by the National "Cellule de Bioéthique".

2.3.7 Cellular internalisation

Before all experiments with human MSCs, a sterilisation step of SPIONs is necessary. For that, an autoclaving treatment is performed at 120°C during 30 min with an autoclave from Advantage Labo (model AL02-07-100). A previous work showed that the physico-chemical properties of SPIONs were not modified after this sterilisation step [24].

SPIONs were internalized in mesenchymal stromal cells (MSCs) with different concentrations of SPIONs: 12.5 µg/mL, 25 µg/mL, 50 µg/mL, 100 µg/mL, 200 µg/mL, 400 µg/mL, 800 µg/mL and 1600 µg/mL. This choice of these concentrations is based on the literature[39]. The solution of SPIONs were incubated with MSCs at 37°C with 5% of CO_2 for 24 hours.
To control the internalisation of SPIONs in MSCs, Prussian Blue staining were realized. MSCs with SPIONs were fixed with Paraformaldehyde (PFA) 4% for 10 min and then immersed in 2% potassium ferrocyanide ($K_4[Fe(CN)_6]$) and 2% HCl for 15 min. They were washed with distilled water and a counterstaining with Kernechtrot (5 min) is realized. After a last wash with distilled water and absolute ethanol, MSCs were mounted in Pertex resin. The stained cells were observed and recorded by light microscopy (DMD108, LEICA).

2.3.8 Mitochondrial activity

Mitochondrial activity in MSCs with SPIONs was evaluated by an MTT (3(4,5-Dimethylthiazol-2-yl)-2-5diphenyltetrazolium bromide) assay. MSCs were placed in wells (5000 cells per well for a volume of

100 µL) with 25 µL of MTT and plates were incubated at 37°C under 5% of CO_2 for 4 hours. MTT has been reduced by dehydrogenase succinate to form formazan crystals.
The supernatant has been removed in order to lyse MSCs with 100 µL of SDS-DMF (80 g of sodium dodecyl sulfate, 200 mL of dimethylformamide, 200 mL of water at pH = 4.7) during 24 hours at 37°C with 5% of CO_2.
Finally, the absorbance was measured at 580 nm thanks to a spectrophotometer (Multiskan Ex from ThermoLabsystem). The results of mitochondrial activity are obtained after 24, 48 and 72 hours of seed.

2.3.9 Relaxometry measurements

Prior to MRI measurements, relaxation properties of SPIONs were evaluated at several values of the magnetic field. The longitudinal ($R_1=1/T_1$) and transverse ($R_2=1/T_2$) proton relaxation rates of water in solutions containing SPIONs at different concentrations (the same concentrations as for cellular internalisation) were measured at 25°C and 0.47T, 0.94T or 1.41T. The proton Larmor frequencies corresponding to these magnetic field values are 20MHz, 40MHz and 60MHz respectively; measurements were made with a Bruker Minispec MQ20, a Bruker Minispec MQ40, and a Bruker Minispec MQ60 respectively. T_1 values were measured with an inversion-recovery pulse sequence and T_2 with a CPMG (Carr-Purcell-Meiboom-Gill) pulse sequence. The relaxivities (longitudinal relaxivity r_1 and transverse relaxivity r_2) were obtained by normalizing the relaxation enhancement of water protons to a millimolar solution of Fe_3O_4. Each relaxivity measurement was realised three times in order to evaluate uncertainties.
^{1}H NMRD (Nuclear Magnetic Relaxation Dispersion) profiles (i.e., longitudinal relaxivities r_1 as a function of the proton Larmor frequency) were also obtained between 5 kHz and 10 MHz on a Stelar Smartracer fast-field-cycling relaxometer (Stelar company, Medde, Italy). Temperature was fixed at 25 °C and T_1 values were measured with an inversion-recovery pulse sequence on the same samples as the ones used at 20MHz, 40MHz and 60MHz.

2.3.10 MRI measurements

MRI imaging were acquired with a Bruker Biospec Advance 24/40 with a 2.34 T magnetic field (100 MHz) equipped with a 5 cm diameter Rapid Biomedical volume resonator. The concentrations of SPIONs which are used for MRI images are the same as the ones used for the cell internalisation and for the relaxometry. Spin echo images were acquired for T_2 contrast with a repetition time of 5 s and an echo time of 50 ms. The total acquisition time for one image was 21 min.

3. Results and discussion

TEM micrographs of each sample, SPIONs_CA1, SPIONs_CA2 and SPIONs_CA3, are shown in Fig.1 (respectively 1a, 1c and 1e) and in Fig.S1 with a higher magnification (respectively S1.a, S1.b and S1.c). For the three samples, SPIONs are spherical and isolated. The size distribution of SPIONs is similar and

narrow for SPIONs_CA1, SPIONs_CA2 and SPIONs_CA3 as shown respectively in Fig 1b, 1d and 1f. The main diameter obtained with these size distributions is, respectively for SPIONs_CA1, SPIONs_CA2 and SPIONs_CA3, 2.62 ± 0.83 nm, 3.30 ± 1.10 nm and 3.80 ± 1.67 nm. These diameters are compared with the hydrodynamic diameter obtained with DLS measurements (symbols on Fig 1b, 1d and 1f). The hydrodynamic diameter is the diameter of the inorganic core plus the diameter of the organic layer plus the solvation sphere. For each sample, there is only one narrow peak which corresponds to a population of size of SPIONs. The hydrodynamic diameter of each SPIONs is larger than that obtained with TEM measurements corresponding to a presence of an organic layer and the solvation sphere. The value of the hydrodynamic diameter is expressed as a number in order to be able to compare it with the diameter obtained by TEM. The hydrodynamic diameter is 7 ± 2 nm for SPIONs_CA1, 9 ± 2 nm for SPIONs_CA2 and 15 ± 4 nm for SPIONs_CA3.

Then, a XRD measurement on each sample is realised to know the crystallographic structure of SPIONs. XRD patterns are shown on supplementary figure S2. Magnetite (Fe_3O_4) and maghemite (γ-Fe_2O_3) crystallise in the same cubic crystal structure ($F_{d\text{-}3m}$). XRD patterns of each sample are compared with a reference pattern of magnetite (COD: 9005836). All the diffraction peaks are indexed with this spinel structure. To confirm the inverse spinel structure, the lattice parameter is calculated for the main peaks on each sample. The lattice parameter of reference Fe_3O_4 is equal to 0.8395 nm and that of reference γ-Fe_2O_3 is equal to 0.8354 nm. The average lattice parameter is equal to 0.8384 nm, 0.8388 nm and 0.8370 nm for SPIONs_CA1, CA2 and CA3 respectively: there are between the lattice parameter of magnetite and maghemite, those are substoichiometric magnetite.

Thanks to the Debye-Scherrer equation, the crystal size can be calculated to compare with the size obtained by TEM images. Indeed, each nanoparticle can be assimilated to one crystal because each nanoparticle is composed of a single domain. To calculate the crystal size, the mean peak of patterns is used, i.e., the (311) peak at around 41.2°. The crystal sizes of SPIONs are respectively 3.5 nm, 3.8 nm and 4.1 nm for CA1, CA2 and CA3. These sizes are in accordance with the diameter measured by TEM.

To confirm the presence of the organic layer, FTIR measurements are realised and shown on supplementary information (Fig. S3). For the three sample, the characteristic vibration bands of citrate are present, i.e., a large band from 3000 cm^{-1} to 3500 cm^{-1} which corresponds to the stretching vibration of O-H of the hydroxyl group in citrate and absorbed water, a band at 2840 cm^{-1} which corresponds to the stretching vibration of CH_2 and the stretching band at 1050 cm^{-1} of C-O of the hydroxyl group. In addition, there are two intense peaks at 1610 cm^{-1} and 1415 cm^{-1} which are respectively the asymmetric and symmetric stretching of carboxylate groups of citrate [40]. To confirm the presence of the carboxylate groups, another band which corresponds to the stretching of C-O in carboxylate is present at 1260 cm^{-1}. These two peaks are shifted compared to the carboxylate bands of a sodium citrate solution (shift of 30 cm^{-1}): this shift is due to the chemisorption of citrate on the surface of the iron oxide (Fig.2). Finally, in the organic part of FTIR spectra (from 1000 cm^{-1} to 4000 cm^{-1}), a last peak is present and corresponds to the stretching of N-H: there is a presence of adsorbed free ammonium.

With FTIR spectra, we can determine the type of iron oxide which is synthesized. Indeed, the FTIR spectrum of magnetite has only one intense peak around 580 cm^{-1} and, for maghemite, there are succession peaks from 400 cm^{-1} to 800 cm^{-1} [41]. In our case, there is a peak at 580 cm^{-1}: the inorganic

core of the three samples is composed of magnetite. However, another peak can be observed which results in a slight oxidation of the magnetite: the inorganic core is so substoichiometric magnetite ($Fe_{3-\delta}O_4$ with δ the deviation from the stoichiometric).

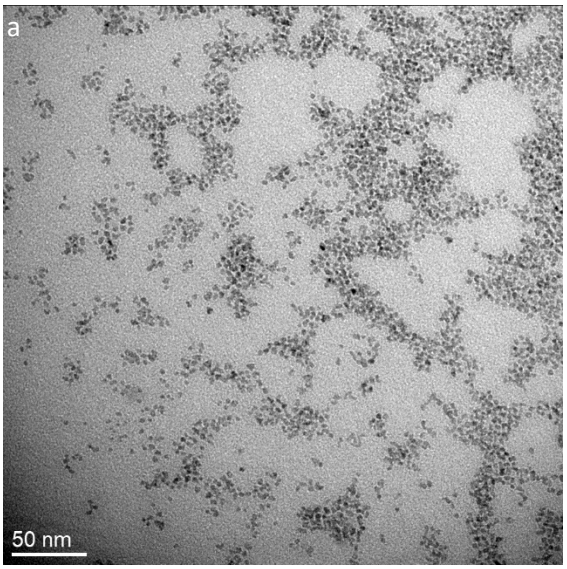

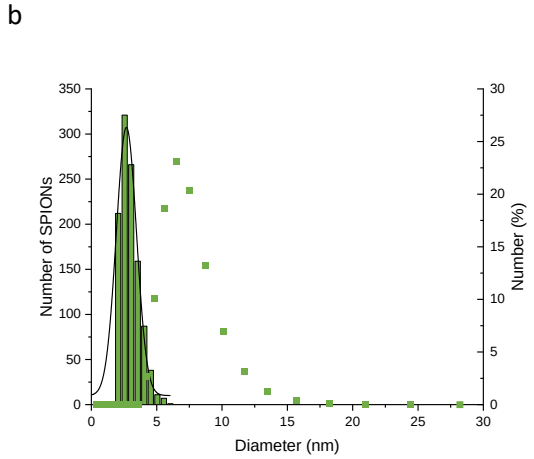

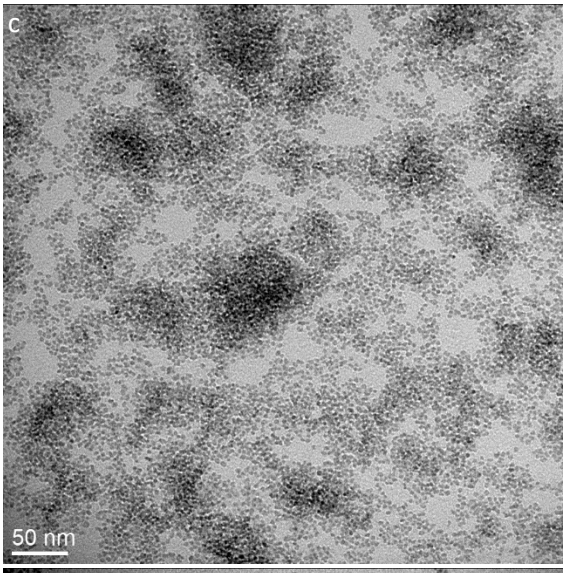

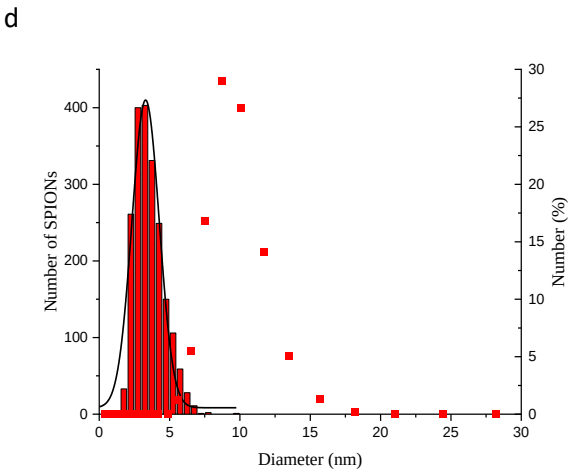

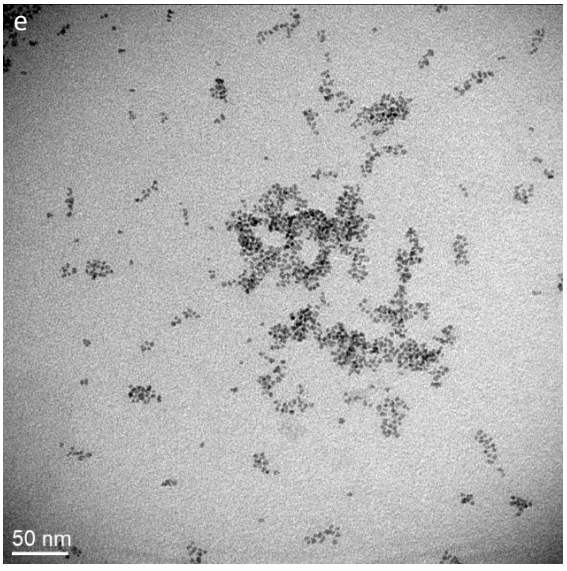

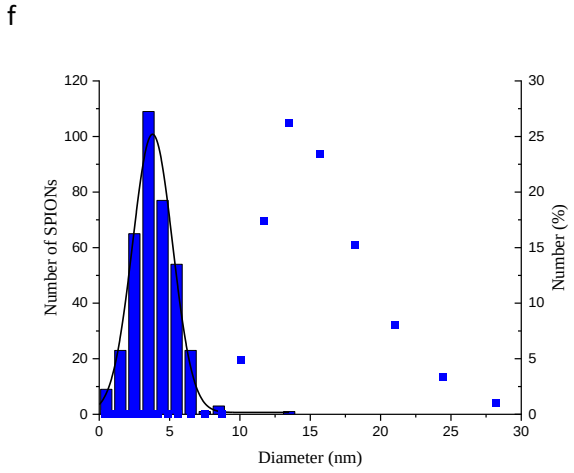

Fig 1: TEM images of iron oxide nanoparticles synthesised by a microwave process with their size distribution (columns) and DLS measurements (symbols). SPIONs_CA1 (a), SPIONs_CA2 (c) and SPIONs_CA3 (e) with their respectively average size equals to 2.62 ± 0.83 nm, 3.30 ± 1.10 nm and 3.80 ± 1.67 nm and a hydrodynamic diameter of 7 ± 2 nm (b), 9 ± 2 nm (d) and 15 ± 4 nm (f).

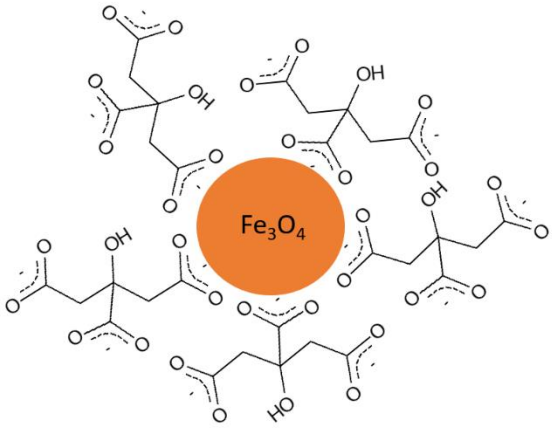

Fig 2: Schema of iron oxide nanoparticle with an organic layer of citrate

The percentage in weight of this organic layer is determined by a thermogravimetric analysis (TGA) and which presents in figure S4. For the three samples of SPIONs, there is the same weight loss. Indeed, three steps of weight loss are present. The first begins at 30°C and finishes at 130°C and it corresponds to the loss of water absorbed. The second stage, from 180°C to 250°C, can be attributed to the decomposition of the citrate. Indeed, if we compare this stage with the decomposition of citrate, the weight loss is similar (Fig S5). Finally, the last stage around 320°C corresponds to the last degradation of citrate. The remaining mass is the mass of iron oxide which is oxidised to hematite (α-Fe_2O_3). The quantity of iron oxide and ligand are detailed in table S1 in supplementary information. For SPIONs_CA1 and SPIONs_CA2, the quantity of ligands and iron oxide are similar but, for SPIONs_CA3, there is an increase of iron oxide so a decrease of ligands. This difference can be explained by the grafting of citrate around the inorganic core. Indeed, citrate can be attached to iron oxide thanks to carboxylate groups. However, with the centrifugation washing, some citrates can be separate to the inorganic core.

Finally, the magnetic properties were studied to determine the magnetic state and the magnetization. In first, a magnetization curve is realised at room temperature to show if a hysteresis is present or not (fig S6). In our case, at 300K, there is no hysteresis and no coercivity: different SPIONs synthesised are in a superparamagnetic state. The superparamagnetic state is a magnetic state where the sum of magnetic moments is null [42,43]. Then, the magnetization saturation is determined thanks to these curves and are equal to 55 $emu.g^{-1}$, 53 $emu.g^{-1}$ and 59 $emu.g^{-1}$ for SPIONs_CA1, CA2 and CA3 respectively. These magnetization saturations are in the same proportion with nanoparticles with the same diameter [44]. To check if iron oxide nanoparticles are in a superparamagnetic state at room temperature, a hysteresis loop is studied at 5K (fig S7). Indeed, at this temperature, iron oxide nanoparticles are in a blocked state which results in an appearance of an opening of the curve. For each sample, a hysteresis is present and confirms the blocked state at 5K. The magnetization saturations obtained at 5K are higher than obtained at 300K due to the blocked state: there are 78 $emu.g^{-1}$, 78 $emu.g^{-1}$ and 75 $emu.g^{-1}$ for CA1, CA2 and CA3 respectively. To determine the transition temperature between the superparamagnetic state and the blocked state (i.e., the blocking temperature called T_B), a ZFC/FC curve is realised (fig S8). T_B is determined thanks to the maximum of the ZFC curve (i.e., the curve from 5K to 300K) and is equal to 14K, 15K and 46K for CA1, CA2 and CA3: the superparamagnetic state is confirmed at room temperature. In addition to that, these curves

correspond to a distribution of T_B and T_B is in function with the diameter of a nanoparticle: if the size increases, the blocking temperature increases too [45]. In our case, for SPIONs_CA1 and SPIONs_CA2, the ZFC/FC curves are narrow so it corresponds to a narrow size distribution: it is adequate to the size distribution obtained by TEM analyses.

After a sterilisation step, a biological study on the behaviour of the iron oxide nanoparticles on cells is realised. For that, different concentrations of SPIONs_CA1, CA2 and CA3 are brought into contact with MSCs. Then, after a coloration of SPIONs and nuclei (with potassium ferrocyanide and Kernechtrot), the internalisation of SPIONs is highlighted (Fig. 3). For the three samples, the internalisation increases with the concentration of SPIONs. For SPIONs_CA3, the internalisation begins at low concentration (12.5 µg SPIONs/mL) without aggregation of the nanoparticles. However, at high concentrations (400, 800 and 1600 µg/mL) for the three samples, few aggregates appear and could induce a cytotoxicity of cells. Indeed, several studies have shown that the low concentrations (from 1 to 100 µg/mL) don't affect the viability and toxicity of various cells such as MSCs [39].

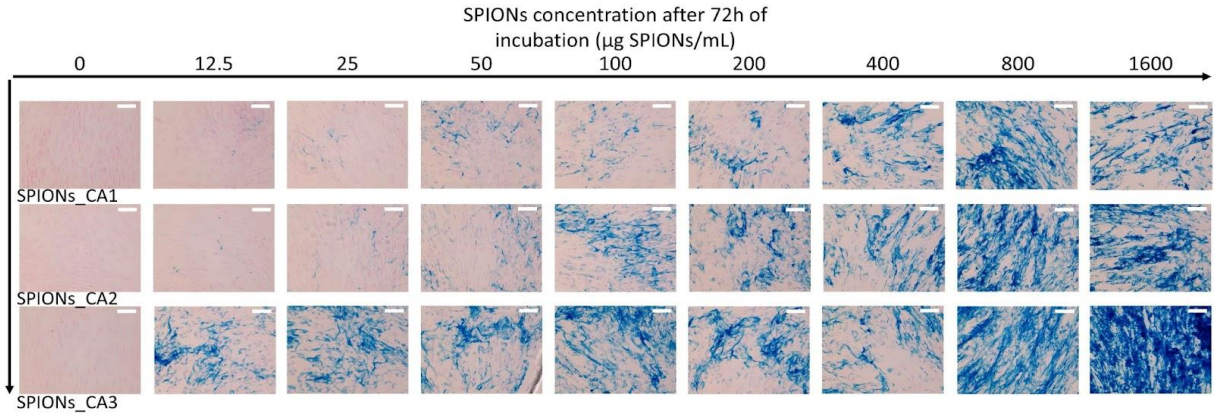

Fig 3: Histological visualisation of human mesenchymal stem cells (MSCs) using Prussian blue staining and Kernechtrot counterstaining. Staining was performed 72 hours after exposure of SPIONs (SPIONs_CA1, SPIONs_CA2 and SPIONs_CA3) with different concentrations (from 100 to 1600 µg SPIONs/mL) (scale bare: 100 µm)

To verify this cytotoxicity, an analysis of the mitochondrial activity is carried out (Fig. 4). The absorbance of the formazan complex (obtained through the reaction between MTT and the succinate dehydrogenase) was collected after 24h, 48h and 72h and compared with a control (black columns) which corresponds to the normal cell viability. For the three samples, there is an increase of the mitochondrial activity over time: this increase is due to the classical cell proliferation. However, for the high concentrations, a decrease in this activity is observed. For SPIONs_CA1, at 1600 µg/mL, the mitochondrial activity is low at 24h, increases at 48h (30% of increase) and decreases at 72h (- 34%): this evolution is likened to a cytotoxicity. For SPIONs_CA2, there is the same behaviour for the high concentrations. Finally, for SPIONs_CA3, there is no difference between the control and the concentrations from 12.5 µg/mL to 200 µg/mL over time. However, for the 400 µg/mL, 800 µg/mL and 1600 µg/mL and only at 24h, the mitochondrial activity is high than the other: for these concentrations, the solution was more viscous than the other and generated a large deposit which was difficult to lyse for analysis. But the presence of this large deposit doesn't induce a cytotoxicity because the mitochondrial activity with the high concentrations is similar to the control. To confirm these results,

a LDH (Lactate DesHydrogenase) test will be released: the same conclusion about the toxicity of different SPIONs was found but the data of LDH are not shown on this work.

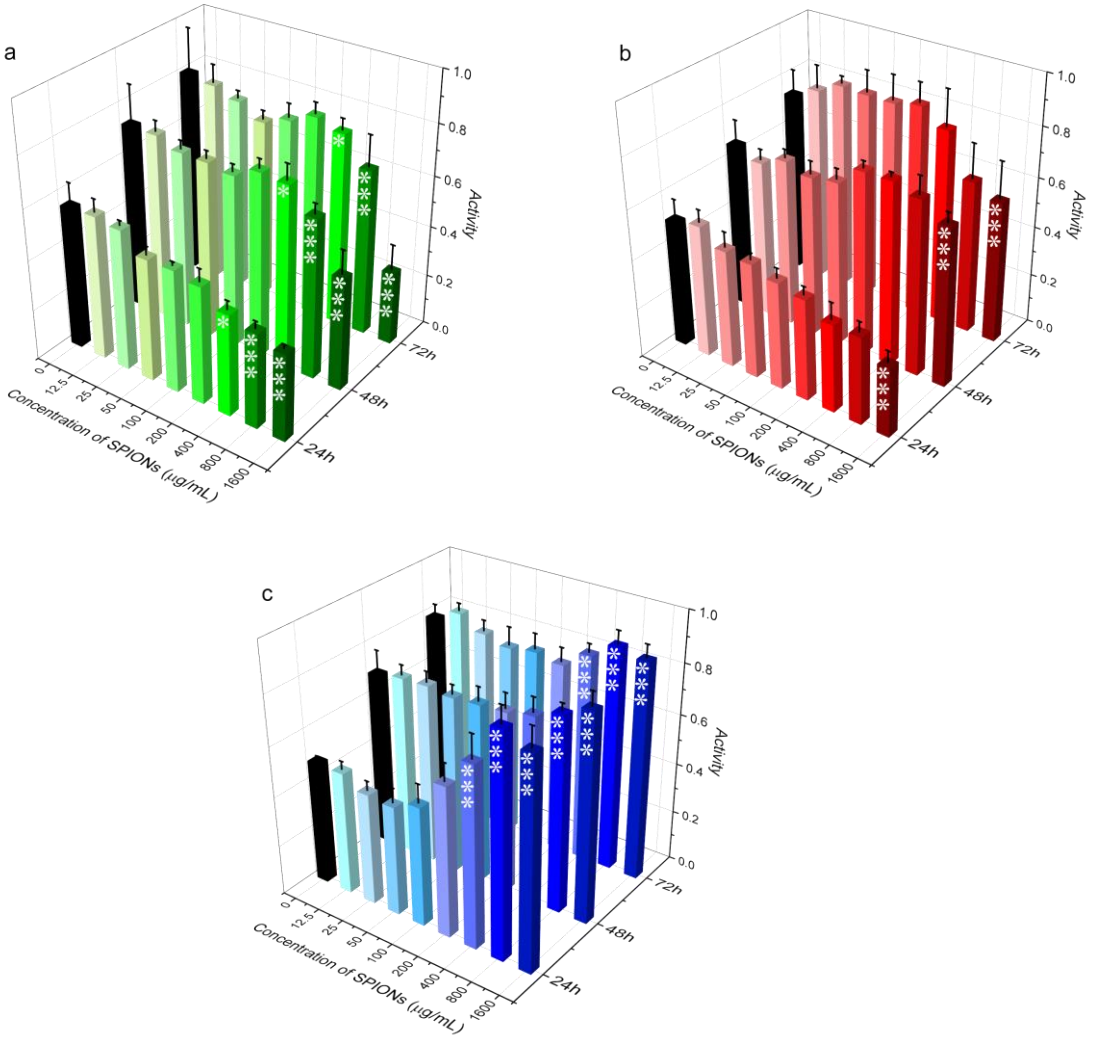

Fig 4: Mitochondrial activity of MSCs with different concentrations of SPIONs collected at 24h, 48h and 72h (SPIONs_CA1 (a), SPIONs_CA2 (b) and SPIONs_CA3 (c)). All comparisons were performed versus the control condition (0) with a 2-ways ANOVA (SPIONs concentrations and time) followed by a Tukey's test. Data are mean ± sd. *p<0.5, **p<0.05 and ***p<0.01. The experiment was carried out five times.

Once the no-toxicity of SPIONs asserted by the first biological tests, their NMR relaxation properties were studied for a potential use as a MRI contrast agent. Longitudinal (R_1) and transverse (R_2) relaxations rates were measured as a function of SPIONs concentration. Relaxivities were obtained from the linear regression of these rates in accordance with the equation $R_i = R_{i,0} + r_i.C$, where $R_{i=1,2}$ is the relaxation rate (s^{-1}) of the aqueous solution, $R_{i=1,2,0}$ (s^{-1}) is the relaxation rate of the aqueous solution without contrast agent, $r_{i=1,2}$ is the relaxivity ($s^{-1}.mmol^{-1}.L$) and C the concentration of the contrast agent ($mmol.L^{-1}$). It characterizes the contribution of the superparamagnetic nanoparticle to the acceleration of water proton relaxation.

Figure 5 shows the transverse relaxation (i = 2) evolution of SPIONs_CA1, CA2 and CA3 at 60 MHz (i.e., 1.4 T) with the concentration. The high values of r_2 obtained from the linear regression show that SPIONs_CA1, CA2 and CA3 are good candidate for negative contrast agents [7,18,46]. The r_2 value is 58 $s^{-1}.mmol^{-1}.L$, 88 $s^{-1}.mmol^{-1}.L$ and 158 $s^{-1}.mmol^{-1}.L$ for SPIONs_CA1, SPIONs_CA2 and SPIONs_CA3 respectively. These values are in accordance with other SPIONs with equivalent diameters [47,48]. From SPIONs_CA1 to SPIONs_CA3, the increase in r_2 values is mainly due to the increase in their hydrodynamic diameters because their saturation magnetizations are of the same order. To complete the relaxation data of these nanoparticles, the r_1 value (longitudinal relaxation) is measured in the same conditions (same concentrations at 60 MHz) and is equal to 22 $s^{-1}.mmol^{-1}.L$, 31 $s^{-1}.mmol^{-1}.L$ and 23 $s^{-1}.mmol^{-1}.L$ for SPIONs_CA1, CA2 and CA3 respectively (Figure S9). The values of $r_{i=1,2}$ are compared with the values of Endorem®, a commercial contrast agent composed of a superparamagnetic iron oxide core (around 5 nm) and an organic layer of dextran. Its hydrodynamic diameter is around 80 to 150 nm [46,49,50] . Endorem® was used as a contrast agent for the lymphatic system in Europe. From literature, Endorem® relaxivity values are between 10 to 24 $s^{-1}.mmol^{-1}.L$ for r_1 and 100 to 158 $s^{-1}.mmol^{-1}.L$ for r_2 at 37°C and 1.5T : these values are in the same order as the relaxivity values of our SPIONs [49,50].

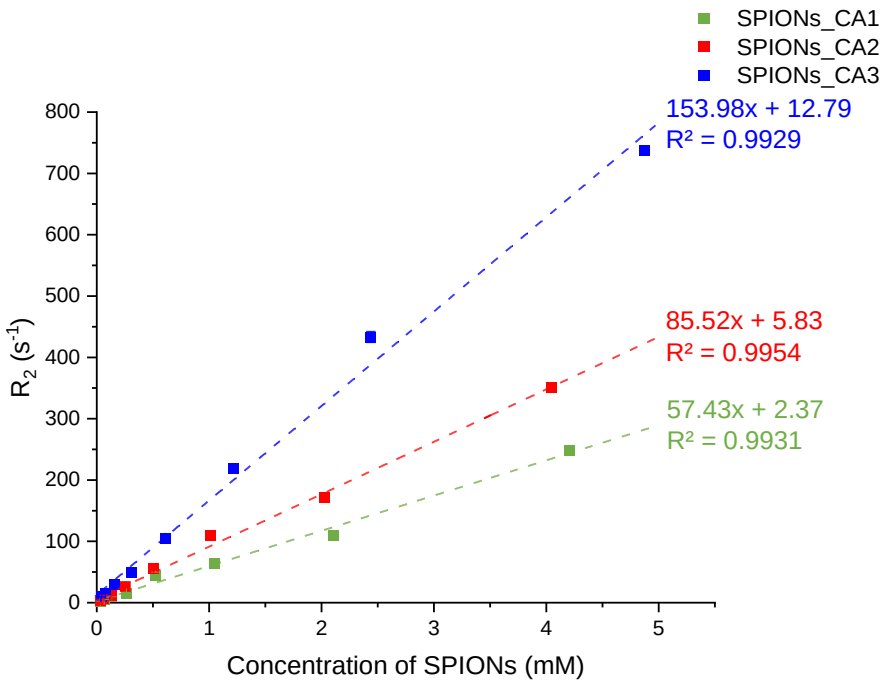

Fig 5: Transverse relaxation rate R_2 (s^{-1}) as a function of SPIONs concentration (mM) at 60 MHz and 25°C. Dashed lines represent the linear regression done for evaluating the transverse relaxivity r_2

These relaxivity results are nicely confirmed by T_2-contrasted Magnetic Nuclear (MR) images shown on Figure 6. Images were obtained at 2.34T on phantoms corresponding to different concentrations of SPIONs (the same as the ones used for MTT tests and relaxometry measurements). The superparamagnetic nanoparticles act by lowering the relaxation time of water protons. When the concentration of SPIONs increases, the signal in the T2-weighted images decreases, as expected.

The NMR relaxometric properties of SPIONs were further investigated by measuring r_1 and r_2 at different values of the magnetic field (Figure S9 to S12). Table 1 summarises the value of $r_{i=1,2}$ of SPIONs_CA1, CA2 and CA3 at 20 MHz (0.47 Tesla), 40 MHz (0.95 Tesla) and 60 MHz (1.41 Tesla). For

the three samples, when the magnetic field increases (i.e., when the frequency increases), the r_2 value increases too but the r_1 value decreases. This behaviour is classical for a superparamagnetic material. To determine if our SPIONs are good candidates for contrast agent for MRI, the ratio between r_2 and r_1 is important (Fig S13) [51]. Indeed, if this ratio is higher to 2, the contrast agent is classified as a negative contrast agent, especially under magnetic fields mostly used in MRI [51]. For SPIONs_CA1 and SPIONs_CA2, the ratio is higher to 2 at 40 MHz (0.95 T) and 60 MHz (1.41 T), these magnetic field values correspond to the ones commonly used in clinical MRI. For SPIONs_CA3, the ratio is higher to 2 under any magnetic fields which are applied (between 3.5 to 6.7): this sample is a very good candidate to be used in a living organism in future works. For comparison, this ratio is between 4 and 15 for Endorem® according to the different authors [49,50].

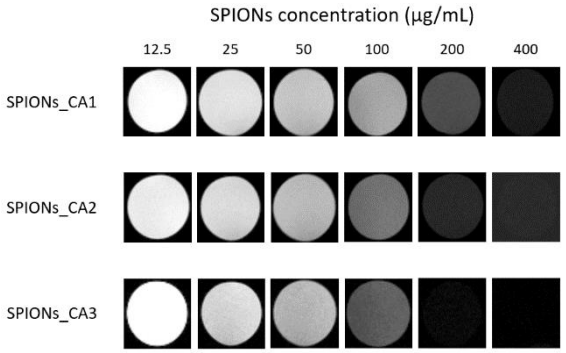

Fig 6: T_2 contrasted MR images at different concentrations of SPIONs under 2.34 Tesla

Table 1: relaxivity $r_{i=1,2}$ ($s^{-1}.mmol^{-1}.L$) of SPIONs_CA1, SPIONs_CA2 and SPIONs_CA3 at different ^1H Larmor frequencies. The relaxivity is obtained by normalizing the relaxation enhancement of water protons to a millimolar solution of SPION. Each relaxivity was realised three times and the average with the standard deviation (sd) are in this table.

	SPIONs_CA1		SPIONs_CA2		SPIONs_CA3	
	r_1	r_2	r_1	r_2	r_1	r_2
20 MHz	23.7 (0.3)	39.3 (0.4)	34.4 (0.3)	59.7 (0.3)	29.0 (0.1)	103.6 (0.7)
40 MHz	23.8 (0.2)	52.5 (0.2)	34.1 (0.2)	78.6 (0.5)	26.5 (0.1)	140.2 (0.7)
60 MHz	21.6 (0.2)	58.3 (0.8)	30.8 (0.1)	87.7 (1.1)	22.8 (0.1)	157.9 (1.2)

Then, NMRD (Nuclear Magnetic Relaxation Dispersion) measurements allowed us to explore a wider range of magnetic fields. Curves describe the evolution of r_1 as a function of the magnetic field expressed in proton Larmor frequency: Figure 7 shows NMRD profiles of SPIONs_CA1, CA2 and CA3 between 10kHz and 60MHz (0.24mT-1.41T) at 25°C. Profiles are characteristic of relaxation induced by superparamagnetic nanoparticles: at low frequency, the relaxation mechanism is driven by the magnetic anisotropy of the nanoparticle, and at high frequency by the diffusion of water molecules at proximity of the magnetic moments of the nanoparticles [44,51,52]. SPIONs_CA1, CA2 and CA3 are the most efficient for water longitudinal relaxation between 20MHz and 40MHz (0.47-0.95T), this magnetic field value correspond to the limit beyond which transverse relaxivity r_2 should be almost constant because the saturation magnetization is reached [53], promising good efficiency as negative contrast agent in MRI. The high field inflection point is correlated to the system dynamics and given by the condition $\omega_H \tau_D = 1$ in which $\tau_D = r^2/D$ with r the hydrodynamic radius of the nanoparticle and

D the relative diffusion coefficient of water. Using D=3.0 10^{-9} $m^2.s^{-1}$, hydrodynamic diameter obtained from the NMRD is equal to 7.4 nm, 6.5 nm and 13.0 nm for SPIONs_CA1, CA2 and CA3 respectively. These diameters are fully consistent with the values obtained by DLS. These fittings are similar to a fitting of a NMRD profile of Endorem®[49].

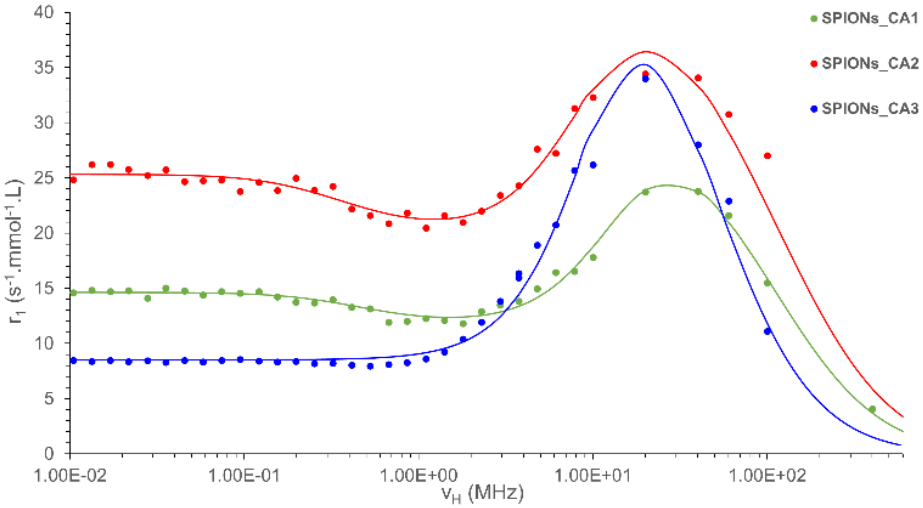

Fig 7: Longitudinal relaxivity (r_1) NMRD profiles of SPIONS between 10kHz and 60MHz (^{1}H Larmor frequency). Continuous lines represent the best fits obtained with the model of Roch et al. [54]

4. Conclusions

In summary, a new method of synthesis of superparamagnetic iron oxide nanoparticles was described in this work. Indeed, these nanoparticles were synthesized by a microwave process and nanoparticles obtained are monodisperse, stable directly in an aqueous medium thanks to the organic layer (citrate). Nanoparticles had a diameter between 2.62 nm to 3.80 nm, had good crystallinity and magnetization saturation higher. These nanoparticles had a goal to use for MRI. For that, several biological tests were carried out to determine the cytotoxicity or not of SPIONs.

The internalisation of SPIONs in MSCs was studied as well as MTT tests: for the three samples, there is no cytotoxicity of MSCs in presence of SPIONs at low concentrations. In addition, the three synthesized SPIONs are a good internalisation in cells, especially SPIONs_CA3 at low concentration: this SPION was a good candidate for the MRI compared to the other. To improve these results, other tests will be carried out such as LDH tests. Thanks to this no toxicity, our nanoparticles are good candidates for MRI. Indeed, with the superparamagnetic state, iron oxide nanoparticles can be used as negative contrast agents. To determine the efficiency for MRI, a preliminary characterization is important: relaxometry. Our nanoparticles have a good transverse relaxivity (r_2), especially SPIONs_CA3 which had a r_2 of 158 $s^{-1}.mmol^{-1}.L$ (in comparison, Endorem®, a negative contrast agent, had a r_2 between 100 to 158 $s^{-1}.mmol^{-1}.L$). However, this value is dependent on the hydrodynamic diameter and the magnetic field. To determine the best conditions for MRI, relaxivity was studied at different magnetic fields, those

used in a classical MRI. NMRD profiles were simulated for the longitudinal relaxivity (r_1) and the same profile that Endorem® was obtained.

Finally, we acquired the first images using MRI which confirmed the good relaxation effects of our nanoparticles.
Future studies will be realised about the NMRD profile for the transverse relaxivity at high magnetic field. Indeed, in the simulation, there is maybe an interaction between the proton of water and nanoparticles which modify the magnetic moment locally and this interaction is neglected in the equation of simulation. In addition to these works, several biological studies will be carried out to determine the exact presence of SPIONs in cells with a cryo-TEM, the colloidal stability of these nanoparticles in blood and their blood compatibility and to determine the cytotoxicity (for example, check the inflammatory nature of the internalisation and the absence of the induction of apoptosis). These different characterizations will allow the use of these nanoparticles in a living organism to determine the behaviour of SPIONs *in vivo*. Finally, these SPIONs could be used in MPI due to their superparamagnetic behaviour and their magnetization. In addition, a study with a coupling of MRI and MPI can be proposed: with this coupling, some diagnostic and anatomic information can be obtained in the same time with a same contrast agent.

There are no conflicts to declare.

Acknowledgements

The authors gratefully acknowledge the "Plateforme de RMN de l'Institut Jean Barriol, Université de Lorraine". In addition, the authors knowledge the center of Microscopy, X-Gamma and Magnetism of Institute Jean Lamour.
Supported by the "SONOMA" project co-funded by "FEDER-FSE Lorraine et Massif des Vosges" 2014-2020, a European Union Program.

Appendix A. Supplementary data

References

[1] C.S.S.R. Kumar, F. Mohammad, Magnetic nanomaterials for hyperthermia-based therapy and controlled drug delivery, Advanced Drug Delivery Reviews, 63 (2011) 789–808.
[2] F. Crippa, L. Rodriguez-Lorenzo, X. Hua, B. Goris, S. Bals, J.S. Garitaonandia, S. Balog, D. Burnand, A.M. Hirt, L. Haeni, M. Lattuada, B. Rothen-Rutishauser, A. Petri-Fink, Phase Transformation of Superparamagnetic Iron Oxide Nanoparticles via Thermal Annealing: Implications for Hyperthermia Applications, ACS Appl. Nano Mater., 2 (2019) 4462–4470.
[3] Y. Jun, Y.-M. Huh, J. Choi, J.-H. Lee, H.-T. Song, S. Kim, S. Yoon, K.-S. Kim, J.-S. Shin, J.-S. Suh, J. Cheon, Nanoscale Size Effect of Magnetic Nanocrystals and Their Utilization for Cancer Diagnosis via Magnetic Resonance Imaging, J. Am. Chem. Soc., 127 (2005) 5732–5733.
[4] T. Vangijzegem, D. Stanicki, S. Laurent, Magnetic iron oxide nanoparticles for drug delivery: applications and characteristics, Expert Opinion on Drug Delivery, 16 (2019) 69–78.
[5] H. Shokrollahi, Contrast agents for MRI, Materials Science and Engineering: C, 33 (2013) 4485–4497.

[6] J.L. Dormann, Magnetic relaxation in fine-particle systems, Advances in Chemical Physics, 98 (1997) 283–494.
[7] A. Alipour, Z. Soran-Erdem, M. Utkur, V.K. Sharma, O. Algin, E.U. Saritas, H.V. Demir, A new class of cubic SPIONs as a dual-mode T1 and T2 contrast agent for MRI, Magnetic Resonance Imaging, 49 (2018) 16–24.
[8] C. Chen, J. Ge, Y. Gao, L. Chen, J. Cui, J. Zeng, M. Gao, Ultrasmall superparamagnetic iron oxide nanoparticles: A next generation contrast agent for magnetic resonance imaging, WIREs Nanomed Nanobiotechnol, 14 (2022).
[9] J. Ward, Use of contrast agents for liver MRI, Radiography, 13 (2007) e54–e72.
[10] X. Yang, G. Shao, Y. Zhang, W. Wang, Y. Qi, S. Han, H. Li, Applications of Magnetic Particle Imaging in Biomedicine: Advancements and Prospects, Front. Physiol., 13 (2022) 898426.
[11] M. Irfan, N. Dogan, O.M. Dogan, A. Bingolbali, Development of Magnetic Particle Imaging (MPI) Scanner for Phantom Imaging of Tracer Agents, IEEE Trans. Magn., 58 (2022) 1–6.
[12] L.L. Israel, A. Galstyan, E. Holler, J.Y. Ljubimova, Magnetic iron oxide nanoparticles for imaging, targeting and treatment of primary and metastatic tumors of the brain, Journal of Controlled Release, 320 (2020) 45–62.
[13] H.M. Jang, M.H. Jung, J.S. Lee, J.S. Lee, I.-C. Lim, H. Im, S.W. Kim, S.-A. Kang, W.-J. Cho, J.K. Park, Chelator-Free Copper-64-Incorporated Iron Oxide Nanoparticles for PET/MR Imaging: Improved Radiocopper Stability and Cell Viability, Nanomaterials, 12 (2022) 2791.
[14] G. Thomas, J. Boudon, L. Maurizi, M. Moreau, P. Walker, I. Severin, A. Oudot, C. Goze, S. Poty, J.-M. Vrigneaud, F. Demoisson, F. Denat, F. Brunotte, N. Millot, Innovative Magnetic Nanoparticles for PET/MRI Bimodal Imaging, ACS Omega, 4 (2019) 2637–2648.
[15] M.-A. Karageorgou, P. Bouziotis, E. Stiliaris, D. Stamopoulos, Radiolabeled Iron Oxide Nanoparticles as Dual Modality Contrast Agents in SPECT/MRI and PET/MRI, Nanomaterials, 13 (2023) 503.
[16] A.G. Roca, L. Gutiérrez, H. Gavilán, M.E. Fortes Brollo, S. Veintemillas-Verdaguer, M. del P. Morales, Design strategies for shape-controlled magnetic iron oxide nanoparticles, Advanced Drug Delivery Reviews, 138 (2019) 68–104.
[17] F. Reyes-Ortega, Á. Delgado, G. Iglesias, Modulation of the Magnetic Hyperthermia Response Using Different Superparamagnetic Iron Oxide Nanoparticle Morphologies, Nanomaterials, 11 (2021) 627.
[18] P. Cheah, T. Cowan, R. Zhang, A. Fatemi-Ardekani, Y. Liu, J. Zheng, F. Han, Y. Li, D. Cao, Y. Zhao, Continuous growth phenomenon for direct synthesis of monodisperse water-soluble iron oxide nanoparticles with extraordinarily high relaxivity, Nanoscale, 12 (2020) 9272–9283.
[19] C.A. Monnier, M. Lattuada, D. Burnand, F. Crippa, J.C. Martinez-Garcia, A.M. Hirt, B. Rothen-Rutishauser, M. Bonmarin, A. Petri-Fink, A lock-in-based method to examine the thermal signatures of magnetic nanoparticles in the liquid, solid and aggregated states, Nanoscale, 8 (2016) 13321–13332.
[20] T. Lam, P. Avti, P. Pouliot, F. Maafi, J.-C. Tardif, É. Rhéaume, F. Lesage, A. Kakkar, Fabricating Water Dispersible Superparamagnetic Iron Oxide Nanoparticles for Biomedical Applications through Ligand Exchange and Direct Conjugation, Nanomaterials, 6 (2016) 100.
[21] M.O. Besenhard, L. Panariello, C. Kiefer, A.P. LaGrow, L. Storozhuk, F. Perton, S. Begin, D. Mertz, N.T.K. Thanh, A. Gavriilidis, Small iron oxide nanoparticles as MRI T_1 contrast agent: scalable inexpensive water-based synthesis using a flow reactor, Nanoscale, 13 (2021) 8795–8805.
[22] S. Slimani, C. Meneghini, M. Abdolrahimi, A. Talone, J.P.M. Murillo, G. Barucca, N. Yaacoub, P. Imperatori, E. Illés, M. Smari, E. Dhahri, D. Peddis, Spinel Iron Oxide by the Co-Precipitation Method: Effect of the Reaction Atmosphere, Applied Sciences, 11 (2021) 5433.
[23] N. Saxena, M. Singh, Efficient synthesis of superparamagnetic magnetite nanoparticles under air for biomedical applications, Journal of Magnetism and Magnetic Materials, 429 (2017) 166–176.

[24] T. Girardet, A. Cherraj, A. Pinzano, C. Henrionnet, F. Cleymand, S. Fleutot, Study of the influence of autoclave sterilization on the properties of citrate functionalized iron oxide nanoparticles, Pure and Applied Chemistry, 93 (2021) 1265–1273.
[25] L. Polito, M. Colombo, D. Monti, S. Melato, E. Caneva, D. Prosperi, Resolving the structure of ligands bound to the surface of superparamagnetic iron oxide nanoparticles by high-resolution magic-angle spinning NMR spectroscopy, Journal of the American Chemical Society, 130 (2008) 12712–12724.
[26] R.K. Kottana, L. Maurizi, B. Schnoor, K. Morris, J.A. Webb, M.A. Massiah, N. Millot, A. Papa, Anti-Platelet Effect Induced by Iron Oxide Nanoparticles: Correlation with Conformational Change in Fibrinogen, Small, 17 (2021) 2004945.
[27] N. Pimpha, N. Woramongkolchai, P. Sunintaboon, N. Saengkrit, Recyclable Iron Oxide Loaded Poly (Methyl Methacrylate) Core/Polyethyleneimine Shell Nanoparticle as Antimicrobial Nanomaterial for Zoonotic Pathogen Controls, J Clust Sci, 33 (2022) 567–577.
[28] N. Ohannesian, C.T. De Leo, K.S. Martirosyan, Dextran coated superparamagnetic iron oxide nanoparticles produced by microfluidic process, Materials Today: Proceedings, 13 (2019) 397–403.
[29] N. Padmavathy, I. Chakraborty, A. Kumar, A. Roy, S. Bose, K. Chatterjee, Fe_3O_4@Ag and Ag@Fe_3O_4 Core–Shell Nanoparticles for Radiofrequency Shielding and Bactericidal Activity, ACS Appl. Nano Mater., 5 (2022) 237–248.
[30] A.H. Hirad, S.A. Ansari, M.A.E. Ali, M.A. Egeh, Microwave-mediated synthesis of iron oxide nanoparticles: Photocatalytic, antimicrobial and their cytotoxicity assessment, Process Biochemistry, 118 (2022) 205–214.
[31] D. Gusain, O.O. Awolusi, F. Bux, Synthesis and characterization of iron oxide/MIL-101 composite via microwave solvothermal treatment, Surface Science, 716 (2022) 121952.
[32] J.-S. Schanche, Microwave synthesis solutions from personal chemistry, Mol Divers, 7 (2003) 291–298.
[33] X. Guo, Y. Ma, Y. Min, J. Sun, X. Shi, G. Gao, L. Sun, J. Wang, Progress and prospect of technical and regulatory challenges on tissue-engineered cartilage as therapeutic combination product, Bioactive Materials, 20 (2023) 501–518.
[34] Y.-D. Xiao, R. Paudel, J. Liu, C. Ma, Z.-S. Zhang, S.-K. Zhou, MRI contrast agents: Classification and application, International Journal of Molecular Medicine, 38 (2016) 1319–1326.
[35] G.J. Strijkers, W.J. M. Mulder, G.A. F. van Tilborg, K. Nicolay, MRI Contrast Agents: Current Status and Future Perspectives, ACAMC, 7 (2007) 291–305.
[36] C.H. Evans, Biochemistry of the Lanthanides, Springer Science & Business Media, 2013.
[37] R. Qiao, C. Yang, M. Gao, Superparamagnetic iron oxide nanoparticles: from preparations to in vivo MRI applications, J. Mater. Chem., 19 (2009) 6274.
[38] S. Laurent, L.V. Elst, R.N. Muller, Superparamagnetic Iron Oxide Nanoparticles for MRI, in: A. Merbach, L. Helm, É. Tóth (Eds.), The Chemistry of Contrast Agents in Medical Magnetic Resonance Imaging, John Wiley & Sons, Ltd, Chichester, UK, 2013: pp. 427–447.
[39] E. Roeder, C. Henrionnet, J.C. Goebel, N. Gambier, O. Beuf, D. Grenier, B. Chen, P.-A. Vuissoz, P. Gillet, A. Pinzano, Dose-Response of Superparamagnetic Iron Oxide Labeling on Mesenchymal Stem Cells Chondrogenic Differentiation: A Multi-Scale In Vitro Study, PLoS ONE, 9 (2014) e98451.
[40] S. Nigam, K. Barick, D. Bahadur, Development of citrate-stabilized Fe3O4 nanoparticles: conjugation and release of doxorubicin for therapeutic applications, Journal of Magnetism and Magnetic Materials, 323 (2011) 237–243.
[41] T.J. Daou, J.M. Grenèche, G. Pourroy, S. Buathong, A. Derory, C. Ulhaq-Bouillet, B. Donnio, D. Guillon, S. Begin-Colin, Coupling Agent Effect on Magnetic Properties of Functionalized Magnetite-Based Nanoparticles, Chem. Mater., 20 (2008) 5869–5875.
[42] L. Néel, Influence des fluctuations thermiques sur l'aimantation de grains ferromagnétiques très fins, (n.d.) 4.

[43] L. Néel, Théorie du traînage magnétique des substances massives dans le domaine de Rayleigh, J. Phys. Radium, 11 (1950) 49–61.
[44] M. Basini, T. Orlando, P. Arosio, M.F. Casula, D. Espa, S. Murgia, C. Sangregorio, C. Innocenti, A. Lascialfari, Local spin dynamics of iron oxide magnetic nanoparticles dispersed in different solvents with variable size and shape: A ^{1} H NMR study, The Journal of Chemical Physics, 146 (2017) 034703.
[45] J.-H. Huang, H.J. Parab, R.-S. Liu, T.-C. Lai, M. Hsiao, C.-H. Chen, H.-S. Sheu, J.-M. Chen, D.-P. Tsai, Y.-K. Hwu, Investigation of the Growth Mechanism of Iron Oxide Nanoparticles via a Seed-Mediated Method and Its Cytotoxicity Studies, J. Phys. Chem. C, 112 (2008) 15684–15690.
[46] S. Tong, H. Zhu, G. Bao, Magnetic iron oxide nanoparticles for disease detection and therapy, Materials Today, 31 (2019) 86–99.
[47] Q.L. Vuong, J.-F. Berret, J. Fresnais, Y. Gossuin, O. Sandre, A Universal Scaling Law to Predict the Efficiency of Magnetic Nanoparticles as MRI T2-Contrast Agents, Advanced Healthcare Materials, 1 (2012) 502–512.
[48] G. Wang, X. Zhang, A. Skallberg, Y. Liu, Z. Hu, X. Mei, K. Uvdal, One-step synthesis of water-dispersible ultra-small Fe3O4 nanoparticles as contrast agents for T1 and T2 magnetic resonance imaging, Nanoscale, 6 (2014) 2953.
[49] S. Laurent, D. Forge, M. Port, A. Roch, C. Robic, L. Vander Elst, R.N. Muller, Magnetic Iron Oxide Nanoparticles: Synthesis, Stabilization, Vectorization, Physicochemical Characterizations, and Biological Applications, Chem. Rev., 108 (2008) 2064–2110.
[50] L.M. Ali, P. Marzola, E. Nicolato, S. Fiorini, M. de las Heras Guillamón, R. Piñol, L. Gabilondo, A. Millán, F. Palacio, Polymer-coated superparamagnetic iron oxide nanoparticles as T2 contrast agent for MRI and their uptake in liver, Future Science OA, (2019) FSO235.
[51] Y. Gossuin, P. Gillis, A. Hocq, Q.L. Vuong, A. Roch, Magnetic resonance relaxation properties of superparamagnetic particles, WIREs Nanomed Nanobiotechnol, 1 (2009) 299–310.
[52] Q.L. Vuong, P. Gillis, A. Roch, Y. Gossuin, Magnetic resonance relaxation induced by superparamagnetic particles used as contrast agents in magnetic resonance imaging: a theoretical review, WIREs Nanomed Nanobiotechnol, 9 (2017).
[53] M.-A. Fortin, Magnetic Nanoparticles Used as Contrast Agents in MRI: Relaxometric Characterisation, in: C.S.S.R. Kumar (Ed.), Magnetic Characterization Techniques for Nanomaterials, Springer Berlin Heidelberg, Berlin, Heidelberg, 2017: pp. 511–555.
[54] A. Roch, R.N. Muller, P. Gillis, Theory of proton relaxation induced by superparamagnetic particles, The Journal of Chemical Physics, 110 (1999) 5403–5411.